JOURNAL OF MATERIALS SCIENCE 12 (1977) 1233–1242

Chemical vapour-deposited silicon nitride

Part 3 *Structural features*

KOICHI NIIHARA, TOSHIO HIRAI
The Research Institute for Iron, Steel and Other Metals, Tohoku University, Sendai, 980, Japan

The massive amorphous and crystalline pyrolytic silicon nitride (Py–Si_3N_4) have been prepared under various conditions of production using $SiCl_4$, NH_3 and H_2. The structural features such as the crystal structure, lattice parameters, grain size, preferred orientation and infra-red absorption are related to the deposition conditions, namely deposition temperature (T_{dep}) and total gas pressure (P_{tot}). The X-ray and electron diffraction data for the crystalline Py–Si_3N_4 show that only α-Si_3N_4 is deposited even at a T_{dep} of 1500° C. The lattice parameter **c** increases with increasing T_{dep} and P_{tot}, while the lattice parameter **a** is independent of T_{dep} and P_{tot}. The parameter **c** depends strongly upon the oxygen content. All the massive Py–Si_3N_4 reveal the strong (1 1 0), (2 1 0) and (2 2 2) orientations, depending upon P_{tot} and T_{dep}. Fine grained Py–Si_3N_4 (about 1 μm) is obtained in the amorphous–crystalline boundary region. The infra-red absorption spectra indicate the stretching vibrations of Si–N compounds. The structure of the massive amorphous Py–Si_3N_4 is also discussed.

1. Introduction

Silicon nitride (Si_3N_4) and silicon carbide (SiC) have been identified by several recent investigations as valuable engineering materials for high-temperature gas turbine applications [1, 2], because of their good oxidation, creep and thermal shock resistance and high hardness and strength at elevated temperatures. It has been reported that these properties are closely related to their structural features [3–8].

Products of Si_3N_4 and SiC can be divided into three groups by the method of production, i.e. reaction-sintering, hot-pressing and chemical vapour-deposition techniques. Usually the reaction-sintering and hot-pressing bodies involve several additives which deteriorate the mechanical strength at elevated temperatures [9, 10]. On the other hand, chemical vapour-deposition can produce highly pure and dense materials which are expected to have superior high-temperature properties. In fact, the chemical vapour-deposited SiC has excellent high-temperature strength up to 1500° C [11–13]. Most of the previous work on Si_3N_4, however, has been carried out on the reaction-sintered and hot-pressed bodies [3–5, 9]. Investigations of chemical vapour-deposited Si_3N_4 (CVD, pyrolytic, Py) are limited to two kinds of thin films, i.e. the amorphous films for semiconductor devices [14, 15] and the crystalline films for protective coatings [16, 17]. Details concerning the methods of production, structures and several properties of massive Py–Si_3N_4 have not been reported so far. This may result from the difficulty in producing massive Py–Si_3N_4.

As reported in Parts 1 and 2 [18, 19], the massive amorphous and crystalline Py–Si_3N_4 with thickness up to 4.6 mm have successfully been prepared at relatively high deposition rates, e.g. 0.73 mm h^{-1} (max.). The deposition rate, density, surface morphology, microstructure and formation mechanism of the massive Py–Si_3N_4 have been related to the deposition conditions such as the deposition temperature and total gas pressure.

This paper deals with the effect of the preparation conditions on the structural features of

the massive Py–Si_3N_4, that is, on the crystal structure, lattice parameters, grain size, preferred orientation and infra-red absorption.

2. Experimental procedure

Amorphous and crystalline Py–Si_3N_4 samples were prepared on a directly heated graphite substrate by pyrolysis of a mixture of NH_3 and $SiCl_4$ carried with H_2. The process used for preparing Py–Si_3N_4 has been fully described in a previous paper [18]. The preparation conditions are, therefore, summarized in Table I. Fig. 1 illustrates the effect of deposition temperature (T_{dep}) and total gas pressure (P_{tot}) on the structure of Py–Si_3N_4 [18]. In Fig. 1, the second notations A and C indicate amorphous and crystalline, respectively.

The density of Py–Si_3N_4 was determined by a displacement technique using toluene and the oxygen content in Py–Si_3N_4 was determined by electron probe microanalysis using fused silica and aluminium single crystals as standard samples, as reported previously [18].

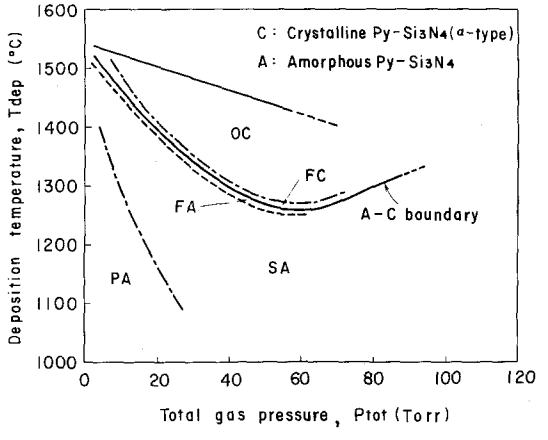

Figure 1 Effect of deposition temperature (T_{dep}) and total gas pressure (P_{tot}) on the structure of Py–Si_3N_4. PA: amorphous deposits with only primary cones, SA: amorphous deposits with primary and secondary cones, FA: amorphous deposits with primary and fine secondary cones, FC: fine grained crystalline deposits, OC: oriented crystalline deposits.

TABLE I The preparation conditions of Py-Si_3N_4

Heating method	Direct heating of graphite substrate
Flow rate ($cm^3\ min^{-1}$)	NH_3 = 60 $SiCl_4$ = 0.8 (in liq.) H_2 = 700
Deposition temperature (° C)	1200–1500
Total gas pressure (Torr)	10–60
Deposition time (h)	0.5–12

The X-ray diffraction patterns of the powdered and bulk (as-deposited) samples of Py–Si_3N_4 prepared under various conditions of production were obtained using a Debye–Scherrer camera with a diameter of 114.6 mm and a diffractometer combined with a scintillation counter and a pulse height analyser. Ni-filtered CuK_α-radiation was employed. The correction of the diameter of the Debye–Scherrer camera was performed using high purity silicon powder as a standard sample. Lattice parameters **a** and **c** were determined by the Nelson–Riley extrapolation method.

The powdered samples were also examined by transmission electron microscopy and selected-area diffractometry. The powdered samples were dispersed in ethyl alcohol and a small amount of the liquid was sprayed onto a Cu-mesh screen. The camera constant of the electron transmission microscope was determined using both *d*-spacings of the hexagonal α-Si_3N_4 and evaporating thin films of gold.

The infra-red absorption spectra for some amorphous and crystalline Py–Si_3N_4 were obtained over the 250 to 3000 cm^{-1} region using a Hitachi grating infra-red spectrometer (model 285).

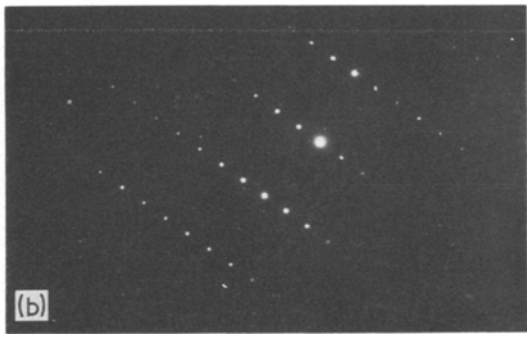

Figure 2 Electron micrograph (a) and electron diffraction pattern (b) of amorphous Py–Si_3N_4 prepared at T_{dep} = 1300° C and P_{tot} = 10 Torr.

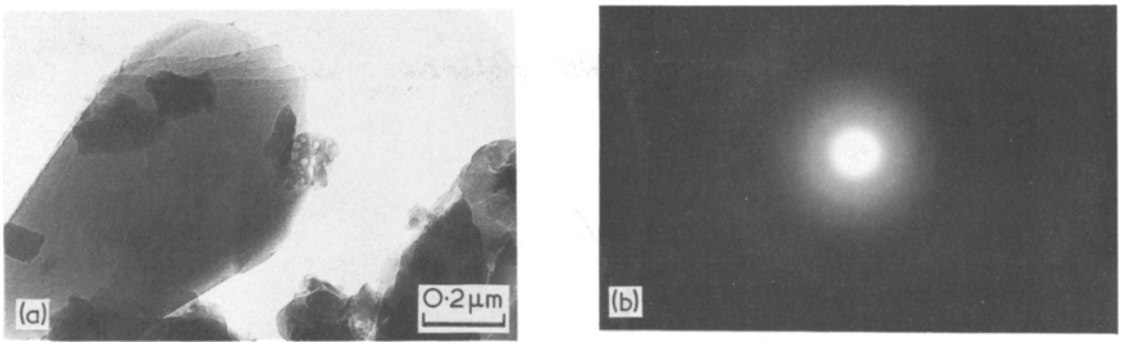

Figure 3 Electron micrograph (a) and electron diffraction pattern (b) of crystalline Py–Si_3N_4 prepared at T_{dep} = 1300° C and P_{tot} = 60 Torr.

These spectra were taken by a Nujol disc method: 1 mg powdered Py–Si_3N_4 was mixed with 350 mg Nujol powder and then pressed into a disc.

3. Results

3.1. Structure

As shown in Fig. 1, structures of Py–Si_3N_4 prepared in this experiment were divided into two types, the amorphous structure in the PA, SA and FA regions and the crystalline structure in the FC and OC regions [18]. Fig. 2 shows an electron micrograph and diffraction pattern of the powdered sample deposited at T_{dep} = 1300° C and P_{tot} = 10 Torr. Two diffused rings were observed in Fig. 2b, indicating the amorphousness of this sample. The X-ray diffraction profile of this sample also presents two broad lines. The outer ring in Fig. 2b corresponds to a spacing of 1.68 ± 0.05 Å and the spacing of the ill-defined inner ring seems to be in the range of 2.4 to 4.6 Å.

Fig. 3 gives the results on the powdered sample prepared at 1300° C and 60 Torr. The electron diffraction pattern (Fig. 3b) was identified as that of an α-Si_3N_4 single crystal whose surface is parallel to the (0 1 3) plane.

The results of X-ray diffraction indicated that all the crystalline Py–Si_3N_4 obtained at 1300 to 1500° C were completely α-Si_3N_4 and no free silicon, β-Si_3N_4 or other silicon compounds were formed (see Fig. 6a).

3.2. Infra-red absorption spectrum

The infra-red spectra of the amorphous and crystalline Py–Si_3N_4 deposited at T_{dep} = 1300° C and P_{tot} = 10 Torr and at T_{dep} = 1300° C and P_{tot} = 60 Torr, respectively, are presented in Fig. 4. The arrows mark the amorphous Py–Si_3N_4 indicated by two broad absorption bands with maxima at approximately 500 and 900 cm^{-1} (Fig. 4a). The broad featureless bands are characteristic of material having low crystallinity. Qualitatively, the absorption peaks were shifted toward lower frequencies with decreasing T_{dep} and with increasing P_{tot}. For example, the amorphous Py–Si_3N_4 prepared at 1100° C and 40 Torr showed two absorption peaks at 480 and 860 cm^{-1}. On the other hand, the infra-red spectrum of the crystalline Py–Si_3N_4 (Fig. 4b) consisted of many sharp absorption bands caused by the splitting of the broad bands in the amorphous Py–Si_3N_4.

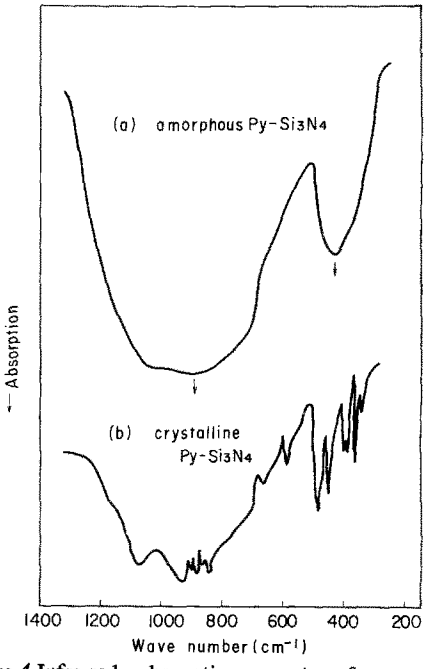

Figure 4 Infra-red absorption spectra for amorphous Py–Si_3N_4 prepared at T_{dep} = 1300° C and P_{tot} = 10 Torr (a) and for crystalline Py–Si_3N_4 prepared at T_{dep} = 1300° C and P_{tot} = 60 Torr (b).

TABLE II Lattice parameters a and c of Py–Si_3N_4 (α-Si_3N_4)

T_{dep} (° C)	P_{tot} (Torr)	Colour*	Density* (g cm^{-3})	Oxygen content* (wt %)	Lattice parameters a (Å)	c (Å)	Unit cell volume, V (Å^3)
Crystalline							
1300	40	Brown	3.16	0.7	7.751 ± 0.002	5.622 ± 0.002	292.6
1300	50	Brown	3.18	0.6	7.752 ± 0.001	5.623 ± 0.001	292.7
1300	60	Purple	3.17	0.4	7.750 ± 0.002	5.625 ± 0.001	292.6
1400	20	White	3.16	1.1	7.752 ± 0.004	5.619 ± 0.003	292.4
1400	30	Brown	3.18	0.6	7.752 ± 0.002	5.623 ± 0.002	292.6
1400	50	Black	3.18	0.3	7.752 ± 0.003	5.627 ± 0.003	292.8
Amorphous							
1300	20	White	2.88	2.1	–	–	–
1400	10	White	2.89	1.6	–	–	–

* [18, 19].

3.3. Effect of T_{dep} and P_{tot} on lattice parameters a and c

Table II gives the relations of the lattice parameters to the density, oxygen content and colour [18, 19] of Py–Si_3N_4 prepared at T_{dep} = 1300 and 1400° C. The oxygen contents of the amorphous Py–Si_3N_4 are higher than those of the crystalline deposits. As shown in Fig. 5a, the oxygen content decreases with increasing T_{dep} and P_{tot}.

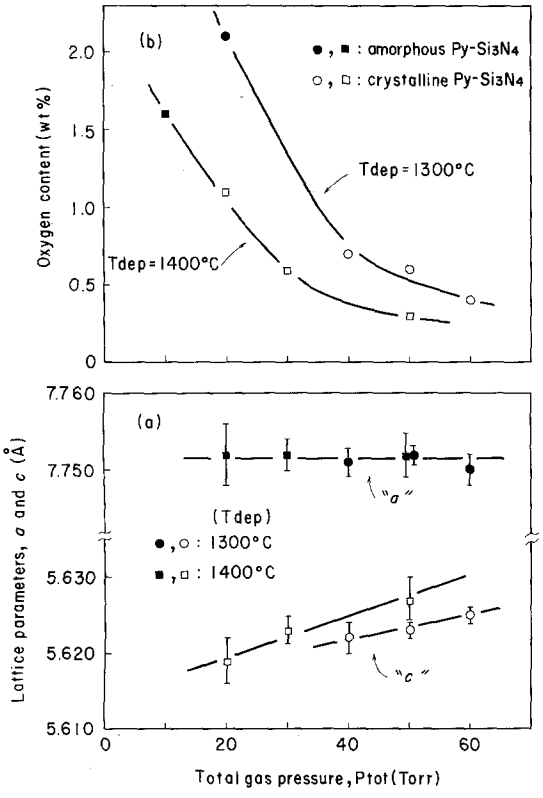

Figure 5 Effect of total gas pressure (P_{tot}) on lattice parameters a and c (a) and oxygen content (b).

Fig. 5b shows the variation of the lattice parameters with P_{tot}. The lattice parameter a is independent of P_{tot}, while the parameter c increases with P_{tot}. From Fig. 5a and b, it is most likely that the variation of the lattice parameters is closely related to the oxygen content.

3.4. Preferred orientation

All the X-ray diffraction patterns of the as-deposited and unground surfaces of the crystalline Py–Si_3N_4 exhibited preferred orientations.

Fig. 6a shows an X-ray diffraction pattern of the powdered sample of Py–Si_3N_4 prepared at T_{dep} = 1300° C and P_{tot} = 60 Torr. The X-ray diffraction profiles of the as-deposited surfaces of the bulk samples of Py–Si_3N_4 obtained at 1300° C and 60 Torr and at 1400° C and 30 Torr are shown in Fig. 6b and c, respectively. Compared with the powder diffraction pattern (Fig. 6a), the X-ray diffraction intensities of the (1 1 0), (2 1 0) and (2 2 2) planes are relatively strong in the sample prepared at 1300° C and 60 Torr (Fig. 6b), and the (2 2 2) plane is preferred at 1400° C and 30 Torr (Fig. 6c). The results on all the Py–Si_3N_4 samples revealed three preferred orientations: the (1 1 0), (2 1 0) and (2 2 2) planes parallel to the deposition surface.

Fig. 7 shows the relationship between P_{tot} and the relative intensity ratio, $[I(2\,2\,2)/I(1\,1\,0)]_{bulk}/[I(2\,2\,2)/I(1\,1\,0)]_{powder}$. The variation of the relative intensity ratio, $[I(2\,2\,2)/I(2\,1\,0)]_{bulk}/[I(2\,2\,2)/I(2\,1\,0)]_{powder}$, with P_{tot} was also similar to that of Fig. 7. As shown in Fig. 7, the preferred orientation of Py-Si_3N_4 depended strongly upon P_{tot}. The (2 2 2) orientation was produced at low P_{tot} and the (1 1 0) and (2 1 0) orientations were observed at high P_{tot}. That is, the (2 2 2) orien-

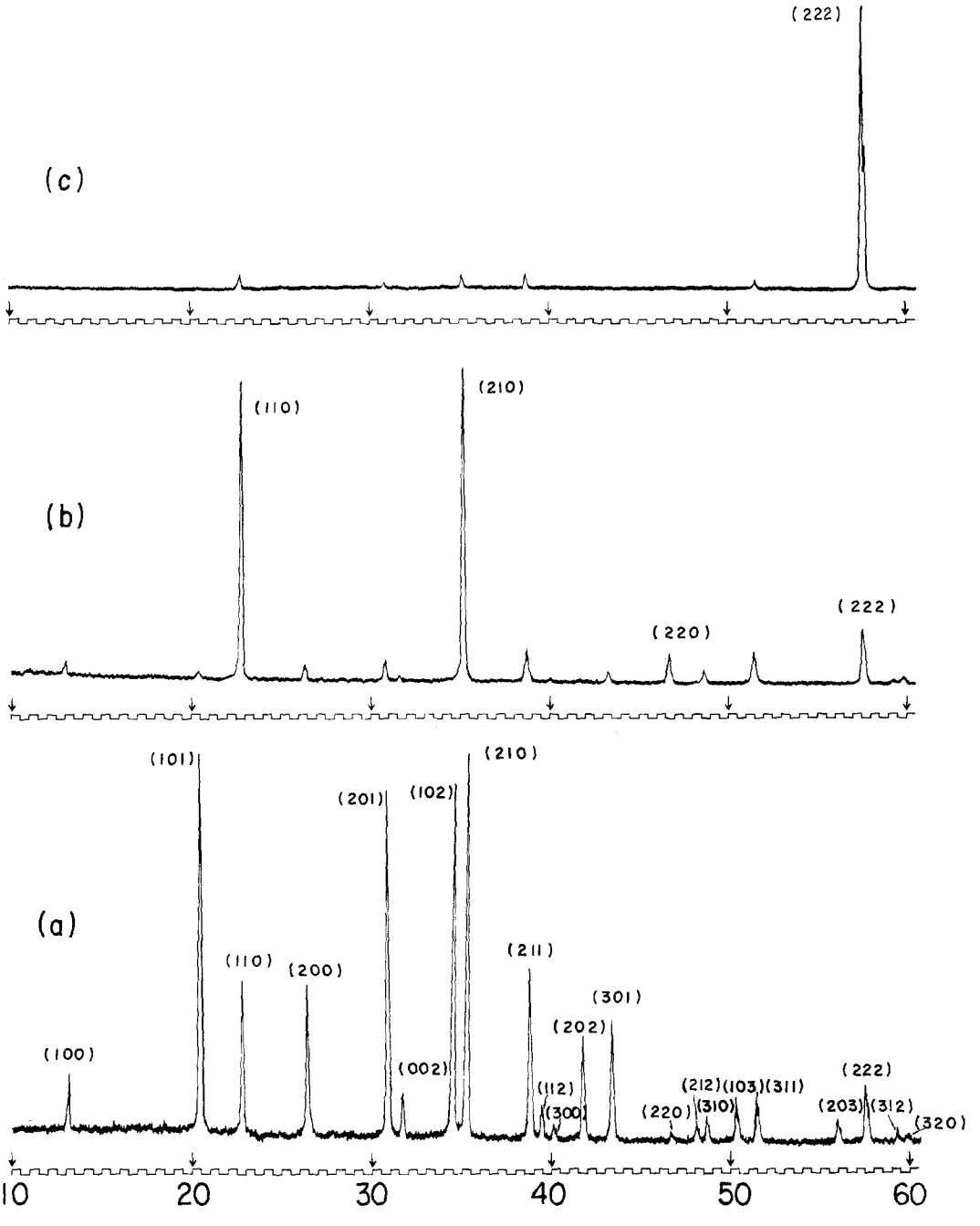

Figure 6 X-ray diffraction patterns of crystalline Py– Si_3N_4 samples. (a) The powdered sample when prepared at $T_{dep} = 1300°$ C and $P_{tot} = 60$ Torr. (b) The as-deposited surface when deposited at $T_{dep} = 1300°$ C and $P_{tot} = 60$ Torr. (c) The as-deposited surface when prepared at $T_{dep} = 1400°$ C and $P_{tot} = 30$ Torr.

tation decreased with increasing P_{tot} and is likely to increase with T_{dep}.

3.5. Grain size

The average grain size of Py–Si_3N_4 was estimated using the electron scanning micrographs of the as-deposited surfaces. The results are summarized in Table III, in which the grain sizes of amorphous Py–Si_3N_4 represent the sizes of the primary and secondary cones. As listed in Table III, the grain sizes of the preferentially oriented Py–Si_3N_4 prepared in the OC region (see Fig. 1) are in excess of 10 μm and those of the deposits obtained in the FC region of the A–C boundary are 1 to 10

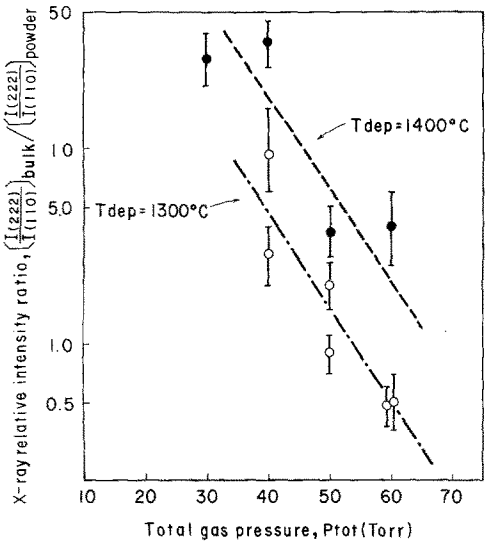

Figure 7 Effect of total gas pressure (P_{tot}) on the preferred orientation for crystalline Py–Si_3N_4 prepared at T_{dep} = 1300 and 1400° C.

TABLE III Cone structure and grain size of amorphous and crystalline Py-Si_3N_4

T_{dep} (° C)	P_{tot} (Torr)	Structure*	Density (g cm^{-3})	Cone or grain size (μm)
1200	10	PA	2.83	30
1200	40	SA	2.60	15
1400	20	FA	2.90	7
1300	40	FC	3.16	1
1300	60	OC	3.17	10
1400	20	FC	3.16	7
1400	50	OC	3.18	15

* PA: amorphous deposits with primary cones, SA: amorphous deposits with primary and secondary cones, FA: amorphous deposits with primary and fine secondary cones, FC: fine grained crystalline deposits, OC: oriented crystalline deposits.

μm. Fig. 8 shows the surface structure composed of fine grains about 1 μm in size as prepared at 1300° C and 40 Torr. It was difficult to obtain the crystalline Py–Si_3N_4 with fine grains of about 1 μm over the entire specimen, because of the partial heterogeneous deposition of both the amorphous and crystalline deposits in the A–C boundary region.

4. Discussion

4.1. Structure of amorphous Py–Si_3N_4

Hu [20] obtained electron diffraction patterns indicating two diffuse rings for the amorphous Py–Si_3N_4 films with thicknesses up to 1.4 μm. The amorphous films were prepared at T_{dep} = 20 to 900° C by pyrolysis of a mixture of NH_3 and SiH_4 and by r.f. and d.c. reactive sputtering of a silicon cathode in pure nitrogen. He reported that a spacing of 1.4 to 1.5 Å calculated from the outer ring corresponded to the distance between neighbouring Si and N atoms, and a spacing of 2.2 to 4.7 Å estimated from the inner ring was a mixed value of a large variety of interatomic distances. Yoshioka *et al.* [21] prepared thin amorphous Py–Si_3N_4 films of extremely short range order by pyrolysis of a mixture of SiH_4, N_2H_4 and H_2 at 550 to 1150° C, and calculated from the transmission electron diffraction patterns that the spacing between the neighbouring Si and N atoms was 1.3 ± 0.05 Å.

Coleman *et al.* [22] calculated the radial distribution function (RDF) from the electron diffraction patterns of thin amorphous Si_3N_4 films prepared from a mixture of NH_3 and SiH_4 at 300° C by a glow discharge. They demonstrated that the first peak in the RDF corresponding to

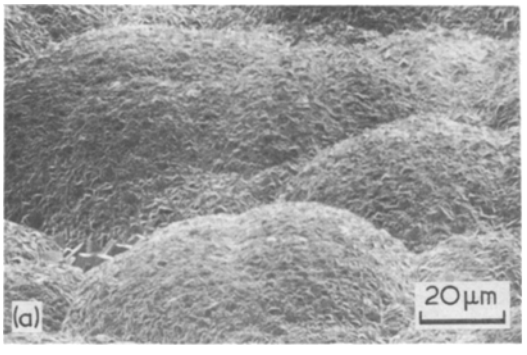

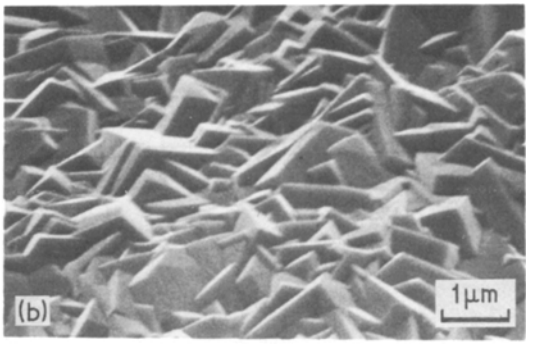

Figure 8 (a) Scanning electron micrograph of the as-deposited surface of Py–Si_3N_4 prepared at T_{dep} = 1300° C and P_{tot} = 40 Torr. (b) Higher magnification of (a).

the spacing between the neighbouring Si and N atoms appeared at 1.70 Å, concluding that the bonding distance and co-ordination of the amorphous Si_3N_4 are the same as those of the crystalline Si_3N_4.

For the massive amorphous Py–Si_3N_4 (4.2 mm thick) obtained in the present work, a spacing of 1.68 ± 0.05 Å calculated from the diameter of the outer ring was larger than the data obtained by Hu [20] and Yoshioka *et al.* [21]. However, the present value shows relatively good agreement with the spacing of the first RDF peak reported by Coleman *et al.* [22] and is also close to the mean interatomic distances between neighbouring Si and N atoms (1.71 to 1.74 Å) of crystalline α-Si_3N_4 [23–25]. Therefore, it seems that there is no remarkable difference in the Si–N spacing between the amorphous and crystalline Si_3N_4 of short range order. A large spacing of 2.4 to 4.6 Å estimated from the ill-defined inner ring in the present experiments can be attributed to the mixing of the spacings of N–N, Si–Si, Si–2nd N, Si–2nd Si and N–2nd N atoms [22].

4.2. Structure of crystalline Py–Si_3N_4

Si_3N_4 has two modifications, designated as α and β, which are considered to be low- and high-temperature phases, respectively. It has been reported that the transformation from α- to β-Si_3N_4 occurs at temperatures above 1400° C [26]. The nitridation of Si powder above 1300° C generally produces a mixture of α- and β-Si_3N_4. On the other hand, Py–Si_3N_4 prepared by a CVD method using various reactants normally showed the α-type structure.

Airey *et al.* [16] prepared the coating of Py–Si_3N_4 using a $SiCl_4 + NH_3 + N_2$ system at 1180 to 1380° C, whereas Berg *et al.* [17] produced the Py–Si_3N_4 coating up to about 0.007 mm thick by pyrolysing a mixture of SiH_4 and NH_3 at 1250° C. Needle-like single crystals of Si_3N_4 were obtained by Bean *et al.* [27] by pyrolysis of $SiH_4 + NH_3$ gases above 1200° C. Galasso *et al.* [28] obtained Si_3N_4 films by pyrolysis of SiF_4 and NH_3 at 1100 to 1550° C. All of these Py–Si_3N_4 were α-Si_3N_4. However, one exception can be found in the results of Nickl and Braunmühl [29], who obtained a mixture of α- and β-Si_3N_4 containing a large amount of free Si by pyrolysis of a $SiCl_4 + N_2 + H_2$ system at 1300° C. In the present experiments on the massive crystalline Py–Si_3N_4, all structural analyses indicated that only α-Si_3N_4 was pyrolytically deposited even at a temperature as high as 1500° C, revealing no experimental evidence as to the formation of the β-type structure.

Wild *et al.* [25], Colquhoun *et al.* [30] and Feld *et al.* [31] have observed that α-Si_3N_4 is, in fact, an oxynitride with a limited range of homogeneity from $Si_{11.5}N_{15}O_{0.5}$ to $Si_{11.4}N_{15}O_{0.3}$ (oxygen: 0.90 to 1.48 wt %), and that β-Si_3N_4 has a stoichiometric composition. Hence they have postulated that the α-Si_3N_4 structure is stabilized by the presence of oxygen.

On the other hand, the experimental results of the structure analyses on the α-Si_3N_4 single crystals [23, 24, 32] and of neutron activation analyses [33–35] indicated that α-Si_3N_4 do not require the presence of oxygen for stabilizing the α-structure.

TABLE IV Literature data of the lattice parameters and oxygen content of various kinds of α-Si_3N_4

Preparation method	Morphology	Oxygen content (wt %)	Lattice parameters* a (Å)	c (Å)	Unit cell volume, V (Å^3)	Reference
CVD of $SiF_4 + NH_3$	Polycrystal	0.30	7.760(1)	5.613(1)	292.7	35
CVD of $SiCl_4 + N_2 + H_2$	Single crystal	0.05	7.818(3)	5.591(4)	295.7	32, 33
CVD of $SiF_4 + NH_3$	Polycrystal	0.3 (Black)†	7.753(1)	5.625(1)	292.8	28
CVD of $SiF_4 + NH_3$	Polycrystal	1.1 (White)†	7.753(1)	5.618(1)	292.4	28
Nitridation of Si	Polycrystal	–	7.752(3)	5.619(1)	292.5	36
Nitridation of Si	Polycrystal	–	7.755(5)	5.616(5)	292.5	26
Nitridation of Si	Polycrystal	–	7.753(4)	5.618(4)	292.4	37
Nitridation of Si	Whisker	–	7.758(5)	5.623(5)	293.1	38
Decomposition of $[Si(NH)_2]_n$	Whisker	–	7.765(1)	5.622(1)	293.5	24
ERDE‡	Needle-like whisker	1.48§	7.7533(8)	5.6167(6)	292.4	25
ERDE‡	Wool-like whisker	1.48§	7.7520(7)	5.6198(5)	292.5	25

* The standard deviation is shown as 7.760(1) for 7.760 ± 0.001.
† These oxygen content were deduced from the result of this work, comparing with the colour of Py–Si_3N_4.
‡ Explosives Research and Development Establishment.
§ $Si_{11.5}N_{15}O_{0.5}$.

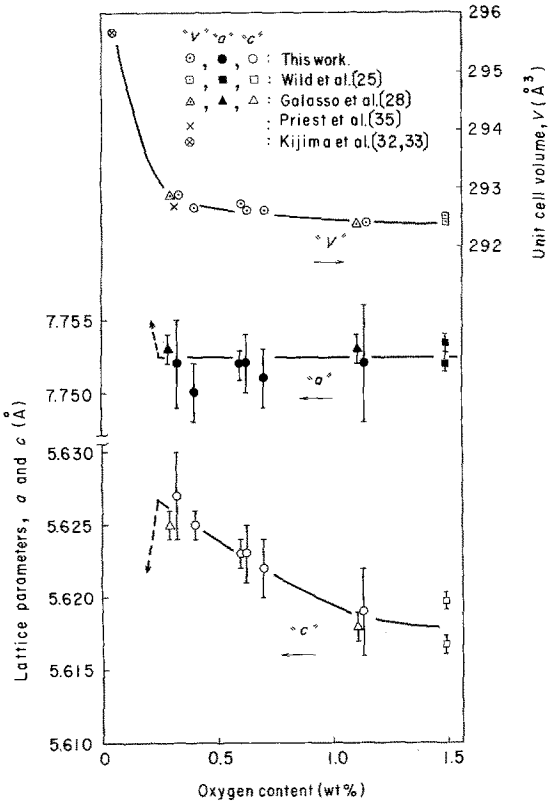

Figure 9 Effect of oxygen content on lattice parameters **a** and **c** and unit cell volume *V*.

Table IV shows the lattice parameters of various kinds of α-Si_3N_4. In the present experiments, the lattice parameters and the oxygen content depended upon T_{dep} and P_{tot} as shown in Fig. 5a and b. Fig. 9 obtained from Fig. 5a and b shows the variation in lattice parameters **a** and **c** with oxygen content. The parameter **c** increases with decreasing oxygen content, while the parameter **a** is almost independent of the oxygen content. Galasso *et al.* [28] obtained the α-Si_3N_4 having different values of the parameter **c**. They considered that the parameter **c** was affected by the oxygen content. The unit cell volume *V* increases with decreasing oxygen content as shown in Fig. 9. For the Py–Si_3N_4 containing 0.3 wt% oxygen, Priest *et al.* [35] reported the lattice parameters **a** and **c** to be 7.760 and 5.613 Å, respectively, which deviated considerably from the results shown in Fig. 9. However, the value for the unit cell volume (292.7 Å^3) was in good agreement with the other experimental data in Fig. 9. In the case of Si_3N_4 containing a very small amount of oxygen (0.05 wt%), the parameters **a** and **c** were 7.818 ± 0.003 and 5.591 ± 0.004 Å, respectively, and the unit cell volume showed a high value as indicated in Fig. 9 [32, 33].

From the above experimental evidence, it may be reasonably considered that α-Si_3N_4 dissolves a considerable amount of oxygen in its own structure although the oxygen is not required for stabilizing the α-structure. Moreover, it is anticipated that the structure of the α-Si_3N_4 containing a considerable amount of oxygen is a structure different from that of the oxygen-free α-Si_3N_4.

4.3. Preferred orientation in crystalline Py–Si_3N_4

Chu *et al.* [15] prepared amorphous Py–Si_3N_4 films using $SiCl_4 + NH_3$ and $SiH_4 + NH_3$ systems, and found that α-Si_3N_4 single crystals were locally formed in the amorphous matrix. The (1 1 0) planes of these single crystals were parallel to the deposition surface. They also reported that the amorphous films were crystallized, upon radiation of an intense electron beam in an electron microscope, into α-Si_3N_4 with an orientation of the (0 0 1) plane. Galasso *et al.* [28] found the pronounced (2 2 2) and (0 0 2) orientations in the α-Si_3N_4 films prepared on a graphite substrate by pyrolysis of a $SiF_4 + NH_3$ system at 1100 to 1550° C and 1 to 10 Torr. Kijima *et al.* [39] prepared α-Si_3N_4 films with the (0 0 2) orientation, using a $SiO_2 + C + N_2$ system at 1400° C on the (1 1 1) plane of Si single crystal. In the literature, however, the relationship between the preferred orientation and the preparation conditions has not yet been clarified. As described above, however, the present experimental results show that all the massive Py–Si_3N_4 of the α-type have the strong orientations of the (1 1 0), (2 1 0) and (2 2 2) planes. Moreover, the preferred orientation is found to depend upon P_{tot} and T_{dep} (see Figs. 6 and 7), i.e. the (1 1 0) and (2 1 0) orientations at high P_{tot} and low T_{dep} and the (2 2 2) orientation at low P_{tot} and high T_{dep}.

In the present Py–Si_3N_4 samples the (0 0 2) orientation was not identified. As reported previously [19], the deposition rate depended strongly upon P_{tot} and T_{dep}. From these results it can be concluded that the (2 2 2) orientation became

more pronounced with increasing deposition rate, and that the (1 1 0) and (2 1 0) orientations became stronger with decreasing deposition rate.

4.4. Infra-red absorption spectrum

The infra-red absorption spectra of the massive amorphous Py–Si_3N_4 samples showed two broad bands (see Fig. 4a), which are similar to the results for the thin amorphous films by Chu *et al.* [15] and Berg *et al.* [17]. The spectra of Mazdiyasni *et al.* [40] on pure α-Si_3N_4 prepared by heating the amorphous polymer $[Si(NH)_2]_n$ at 1200 to 1300° C for more than 2 h are in good agreement with those with a large number of relatively sharp peaks for the massive crystalline Py–Si_3N_4 samples in the present experiment. In their work, the absorption bands at 850 to 1000 cm^{-1} and 300 to 600 cm^{-1} were found to compare favourably with the absorption frequencies of the Si–N compounds involving Si–N–Si, Si_2–N–Si and $(-SiN-)_n$ units with antisymmetrical Si–N stretching frequencies of 900 to 1000 cm^{-1} and symmetrical stretching frequencies of 400 to 600 cm^{-1}. In this work, the absorption bands (570 and 440 cm^{-1} [40]) from β-Si_3N_4 were not identified.

5. Conclusion

(1) The spacing between neighbouring Si and N atoms for the massive amorphous Py–Si_3N_4 was 1.68 ± 0.05 Å which matches fairly well with that for the crystalline α-Si_3N_4 of short range order.

(2) The crystal structure of the massive crystalline Py–Si_3N_4 was α-type. The lattice parameter **c** of Py–Si_3N_4 increased with increasing T_{dep} and P_{tot}, while the parameter **a** was almost independent of the preparation conditions. The lattice parameter **c** increased with decreasing oxygen content, but the parameter **a** was not affected.

(3) For crystalline Py–Si_3N_4, strong preferred orientations of (1 1 0), (2 1 0) and (2 2 2) planes were observed. The (2 2 2) and the (1 1 0) and (2 1 0) orientations were predominant at low P_{tot} and high T_{dep} and at high P_{tot} and low T_{dep}, respectively. The (2 2 2) orientation increased with increasing deposition rate.

(4) The grain size of Py–Si_3N_4 was influenced by P_{tot} and T_{dep}. It was approximately 1 μm in the A–C boundary region and above 10 μm in the OC region.

(5) The infra-red absorption spectrum for the massive amorphous Py–Si_3N_4 consisted of two broad bands having maxima at about 500 and 900 cm^{-1} presumably due to the symmetrical stretching vibration and the antisymmetrical stretching vibration of Si–N compounds, respectively. For the massive crystalline Py–Si_3N_4, the broad bands observed in the amorphous Py–Si_3N_4 were split into many sharp bands.

Acknowledgements

The authors would like to express their appreciation to Dr M. Kikuchi for carrying out the infra-red absorption analysis. This research was supported in part by the scientific research fund from the Ministry of Education, Contract Nos. 040715 and 075078.

References

1. A. F. McLEAN, *Bull. Amer. Ceram. Soc.* **52** (1973) 464, 482.
2. R. A. ALLIEGRO and S. H. COES, American Society of Mechanical Engineers Paper 72-GT-20, March 1972.
3. B. F. JONES and M. W. LINDLEY, *J. Mater. Sci.* **10** (1975) 967.
4. G. G. DEELEY, J. M. HERBERT and N. C. MOORE, *Powder Met.* 8 (1961) 145.
5. R. F. COE, R. J. LUMBY and M. F. PAWSON, "Special Ceramics 5", edited by P. Popper (British Ceramic Research Association, Stoke-on-Trent, 1968) p. 361.
6. E. H. VOICE and V. C. SCOTT, *ibid,* p. 1.
7. C. W. FORREST, P. KENNEDY and J. V. SHENNAN, *ibid,* p. 99.
8. S. PROCHAZKA and R. J. CHARLES, *Bull. Amer. Ceram. Soc.* **52** (1973) 885.
9. S. WILD, P. GRIEVESON, K. H. JACK and M. J. LATIMER, "Special Ceramics 5", edited by P. Popper (British Ceramic Research Association, Stoke-on-Trent, 1968) p. 377.
10. R. A. ALLIEGRO, D. W. RICHERDSON, M. L. TORTI, M. E. WASHBURN and G. Q. WEAVER, *Proc. Brit. Ceram. Soc.* **22** (1973) 129.
11. V. CHATFIELD, *Mat. Eng.* 8 (1974) 44.
12. R. E. ENGDAHL, Report 740184 presented at Automobile Engineering Congress, Detroit (February 1974).
13. J. R. WEISS and R. J. DIEFENDORF, "Chemical Vapour Deposition, Fourth International Conference" edited by G. F. Wakedfield and J. M. Blocher, Jun. (Electrothermics and Metallurgy Division, The Electrochemical Society, New Jersey, 1973) p. 488.
14. C. R. BARNES and C. R. GEESNER, *J. Electrochem. Soc.* **107** (1960) 98.
15. T. L. CHU, C. H. LEE and G. A. GRUBER, *ibid* **114** (1967) 717.
16. A. C. AIREY, S. CLARKE and P. POPPER, *Proc. Brit. Ceram. Soc.* **22** (1973) 305.

17. D. BERG, D. W. LEWIS, T. W. DAKIN, D. E. SESTRICH and J. N. ESPOSITO, Westinghouse Research Laboratories Technical Report AFML-TR-66-320-Part II (November 1967).
18. K. NIIHARA and T. HIRAI, *J. Mater. Sci.* **11** (1976) 593.
19. *Idem, ibid* **11** (1976) 604.
20. S. M. HU, *J. Electrochem. Soc.* **113** (1966) 693.
21. S. YOSHIOKA and S. TAKAYANAGI, *ibid* **114** (1967) 962.
22. M. V. COLEMAN and D. J. D. THOMAS, *Phys. Stat. Sol.* **25** (1968) 241.
23. I. KOHATSU and J. W. McCAULEY, *Mat. Res. Bull.* **9** (1974) 917.
24. R. MARCHAND, Y. LAURENT, J. LANG and M. Th. Le BIHAN, *Acta Cryst.* **25** (1969) 2157.
25. S. WILD, P. GRIEVESON and K. H. JACK, "Special Ceramics 5", edited by P. Popper (British Ceramic Research Association, Stoke-on-Trent, 1972) p. 385.
26. D. S. THOMPSON and P. L. PRATT, "Science of Ceramics, Vol. 3", edited by G. H. Stewart (Academic Press, New York, 1967) p. 33.
27. K. E. BEAN, P. S. GLEIN and R. L. YEAKLEY, *J. Electrochem. Soc.* **114** (1967) 733.
28. F. GALASSO, L. KUNTZ and W. J. CROFT, *J. Amer. Ceram. Soc.* **55** (1972) 431.
29. J. J. NICKL and C. V. BRAUNMÜHL, *J. Mater. Sci.* **37** (1974) 1317.
30. I. COLQUHOUN, S. WILD, P. GRIEVESON and K. H. JACK, *Proc. Brit. Ceram. Soc.* **22** (1973) 207.
31. H. FELD, P. ETTMAYER and L. PETZENHAUSER, *Ber. Dt. Keram. Ges.* **51** (1974) 127.
32. K. KATO, Z. INOUE, K. KIJIMA, I. KAWADA, H. TANAKA and T. YAMANE, *J. Amer. Ceram. Soc.* **58** (1975) 90.
33. K. KIJIMA, K. KATO, Z. INOUE and H. TANAKA, *J. Mater. Sci.* **10** (1975) 362.
34. A. J. EDWARDS, D. P. ELIAS, M. W. LINDLEY, A. ATKINSON and A. J. MOULSON, *J. Mater. Sci.* **9** (1974) 516.
35. H. F. PRIEST, F. C. BURNS, G. L. PRIEST and E. C. SKAAR, *J. Amer. Ceram. Soc.* **56** (1973) 395.
36. H. SUZUKI, *Bull. Tokyo Inst. Technol.* **54** (1963) 163.
37. S. N. RUDDLESDEN and P. POPPER, *Acta Cryst.* **11** (1958) 465.
38. W. D. FORGENG and B. F. DECKER, *Trans. Met. Soc. AIME* **212** (1958) 343.
39. K. KIJIMA, N. SETAKA, M. ISHII and T. TANAKA, *J. Amer. Ceram. Soc.* **56** (1973) 346.
40. K. S. MAZDIYASNI and C. M. COOKE, *ibid* **56** (1973) 628.

Received 16 July and accepted 27 July 1976.